This study was supported by the National Research, Development and Innovation Office (NKFIH-124636) to Viktor Jáger

Summary of research objectives and the difficulties

The aim of the project was to create a methodology to separate ancient microbial structures in geological samples from abiotic (biomimetic) ones. The initial goals were 1.) to create/use a computer program for the differentiation of the bacteriogenic and biomimetic structures and 2.) to synthesize biomimetic structures under laboratory conditions. The latter aim of the project had to be cancelled due to the leave of our colleague Roland Farkas. To confirm the relevance of the 2.) goal of the project we performed the literature review (Bianciardi et al., 2014). At the same time, Béla Frigyik failed to deliver the computer program. However, with the help of Zsuzsanna Márton we could find an appropriate sofware for the fractal analysis of the questioned structures.

Our next goal was to found geological formations with biomimetic and bacteriogenic structures. This required the following analysis: petrography, total organic carbon measurements, scanning electron microscopy, energy dispersive X-Ray spectroscopy, X-ray powder diffraction, Raman spectroscopy, trace element analysis, nucleic acid isolation, fractal dimension analysis, directional analysis, sulfur isotope analysis. K/Ar radiometric dating, fluid inclusion petrography and microthermometry also were carried out to better understand the geological background.

Basalt fragments and sulphide minerals (pyrite and marcasite) were analysed by scanning electron microscopy and energy dispersive X-Ray spectroscopy (SEM-EDS). These minerals and the basalt were placed into two springs located in the Mecsek Mts. and left there for 6 months. Genus-level metagenomic classification was done on the collected water samples from these springs. Based on these results, sulphur- and iron-oxidizing organisms were presented in the spring water during the sampling (Pécs-Vasas and Komló-Mecsekjánosi). The initial aim of this was to identify bacterial activity and follow up the textural and chemical changes on the surfaces of these fragments by using SEM-EDS. However, because these samples were stolen from the springs two times after each other this part of the research had to be neglected.

We collected geological samples from the eastern part of Mecsek Mts. and from the Geresd-Hills. We aimed to collect samples with possible ancient bacterial and biomimetic structures. The main conclusions of the project were made based on the analysis of these samples. Two manuscripts were submitted to different d1 journals. The publication of the submitted manuscripts are delayed due to COVID-19 and the above described difficulties of the project. One of the manuscript is under review at Palaeo3 journal (manuscript number: PALAEO-D-21-00261). The other manuscrip is under correction based on the review of the Journal of the Geological Society (manuscript number: jgs2021-025). Both manuscripts and related data are available upon request.

Main results of the research

1. Based on their helical morphology and stalk parameters, iron oxidizing bacteria found in the injection dykes of Ófalu are strongly resembles to recent *Gallionella* and *Mariprofundus* spp.

2. We confirmed the conversion of bacterial ferrihydrite to microcrystalline hematite. The microcrystalline (0.5-1μm) occurrence of hematite can be used as an indicator for ancient bacterial activity.

3. The recent *Gallionella* and *Mariprofundus* spp. have characteristic aerotactic cell movements. These cell movements were identified by directional analysis of mineralized stalks on certain parts of the rock, which can be used as indicators for ancient bacterial activity.

4. Fractal analysis was used to separate bacterial structures (Df ~1.9) from morphologically similar but abiogenic (Diffusion-Limited Aggregation) structures (Df ~1.7).

5. This is the first detection in Hungary of structures with possible bacterial origin from intrusive basalt that solidified in the calcareous mud. Several microtubular structures occur in the altered volcanic glass with an uniform width of 1.5 μm and up to 200 μm in length, without intersecting one other. The microtubules are rarely bifurcate and curvy. These structures with constant and nearly bacterial cell-size diameter highly resemble bacterial tunneling structures.

6. Biomimetic dendritic, filamentous and periodic precipitation structures (DLA-structures, abiogenic filaments, „chemical stromatolites") has been identified and analysed that were consisted of hydrothermally altered basalt (i) and crustacean coprolites (ii) from the Eastern-Mecsek Mts.

6.1 At the *Pusztakisfalu-section*, slow diffusion of low temperature hydrothermal fluids occurred (along the fissures of intrusive pillows and the cracks of intrusive hyaloclastites), basaltic glass alteration into amorphous palagonite and smectite show periodic precipitation patterns and chemical garden-like structures. The hydrothermal alteration of the basaltic material into these fibrous, dendritic and periodic structures are clearly traceable in the calcite matrix

6.2 At the *Jánosi-puszta section*, besides the hydrothermal alteration structures of the basaltic hyaloclastite, hydrothermal decomposition of amorphous crustacean coprolites into smectite also resulted in similar bacteriomimetic, filamentous structures, where the large surface area of the parallelly formed smectitic filaments likely played a role in the passive sorption of iron hydroxide released from the hydrothermally altered hyaloclastite.

RESEARCH REPORT

A. Comparisons of recent Fe-oxidizing bacteria with Cretaceous Fe-oxidizing bacteria and with morphologically similar, but abiogenic Fe-oxyhydroxide structures

Unambiguous and well-preserved microfossils of the mineralized stalks and sheats of Fe-oxidizing bacteria (FeOB) are very scarce in the geological record. Helical stalk morphology is the most characteristic and distinctive feature of some recent Fe-oxidizing bacteria, such as *Mariprofundus* and *Gallionella* (Li et al., 2020). The distinctive helical morphology of FeOB results from cell rotation during growth (Chan et al., 2011). Filaments with morphologies and structures similar to those formed by recent FeOB of *Gallionella* and *Mariprofundus* were found in Carboniferous (Boyce et al., 2003) and Cambrian (Little et al., 2004) rocks, associated with ancient hydrothermal vent sites. Paleoproterozoic possibly FeOB microfossils were reported by Edwards et al. (2012) from shallow marine chert and sedimentary phosphate, and most recently from shallow marine ironstones by Lin et al. (2019).

Oxides on the stalks of recent FeOB sheaths have been identified as ferrihydrite (Kasama and Murakami, 2001; Kennedy et al., 2003; Rubin-Blum et al., 2014). Recent microbial ferrihydrite can form in any environment where Fe^{2+} -bearing waters come into contact with O_2 (Konhauser, 1998). Deposits of ferric hydroxide-rich muds with microbial mats have been described from several submarine hydrothermal sediments. In shallow marine environment, on the island of Santorini, ferric hydroxide-rich surface layers of sediments can be found around the exhalative zone of a shallow marine hydrothermal vent, where *Gallionella ferruginea* occurs abundantly (Holm, 1987; Cronan et al., 2000; Hanert, 2002; Varnavas and Cronan, 2005). In deep-sea environments of the Pacific Ocean, hydrothermal sediments contain iron oxidizers, and ferric iron deposited just around the vents at the Larson's Seamounts on the Juan de Fuca Ridge (Hrischeva and Scott, 2007), at the Sea Cliff hydrothermal field on the northern Gorda Ridge (Zierenberg and Schiffman, 1990), at the Loihi Seamount of Hawaii (Emerson and Moyer, 2002), and at the Lau Basin near the Australian-Pacific plate boundary (Li et al., 2020).

Ancient analogues of recent marine hydrothermal Fe oxide hydroxide deposits where microbial iron oxidation occured are, for example, the Paleoproterozoic Banded Iron Formations (BIFs) (Little et al., 2004; Kappler et al., 2005; Edwards et al., 2011). The great oxidation event in the beginning of the Paleoproterozoic era likely coincides with the flourishing of FeOB following a period when Earth's oceans were thought to be largely anoxic and rich in Fe^{2+} (Emerson et al., 2010).

Injection dykes are sedimentary dykes, filled with fluidized sediments (Montenat, et al., 2007). The formation of injection dykes results from the hydrofracturing of a hard substrate and infilling of the fractures by overpressured sediments when seismic shocks occur in a fault zone. Consequently, injection dykes are good indicators of palaeoseismic activity (Flügel, 2004; Montenat et al., 2007). In the Geresd Hills in southwest Hungary, at the prominent tectonic belt of the Mecsekalja Zone, previous studies documented a fracture system that is

filled with multiple generations of carbonate veins, including a fracture system filled with a curious, micro-crystalline hematitic carbonate material (Dabi et al., 2011; 2013). The formation of this hematitic carbonate (hereinafter referred to as hematitic carbonate dykes) was linked to an Early Cretaceous volcanic event that resulted in the emplacement of numerous basaltic dykes and sills in this region (Dabi et al., 2011; 2013). However, a detailed understanding of the formation mechanism and the origin of the hematitic carbonate material, as well as its relationship with the Early Cretaceous igneous activity is missing.

The present study provides an in-depth analysis of these unusual hematitic carbonate dykes and is the first to document microtextural features that suggest the activity of ancient Fe-oxidizing bacteria in these rocks. Furthermore, this study describes a fractal dimension- and directional analysis-based methodology that can be applied to help differentiate biotic and abiotic filamentous structures in ancient rocks. Our investigations suggest that the hematitic carbonate dykes were formed due to earthquake events with co-occurring seismic shaking effects, where overpressured (fluidized) sediments were drawn into the fissures of the metamorphic basement and these sediments later lithified as injection dykes.

Geological setting

The investigated area in SW Hungary is part of the Tisza Mega-unit (TMU). The hematitic carbonate dykes were investigated in an outcrop in the Gresed Hills near Ófalu in an east–west oriented tributary valley of the Goldgrund valley (46°13’00 N; 18°33’32 E). This section lies along a transform tectonic belt (Mecsekalja Zone) which is a 1.5-km-wide, NE–SW trending tectonic zone. The Mecsekalja Zone (MZ) includes a very heterogeneous metamorphic rock assemblage displaying intense folding and Early Variscan (Carboniferous) greenschist facies mylonitisation (M. Tóth et al., 2005).

In the studied section, the Paleozoic metamorphic rocks of the Ófalu Formation are exposed on the surface, which are mainly strongly foliated and mylonitised orthogneiss varieties containing lens-like bodies of serpentinite, metabasite and marble. The trend of their foliation is NE–SW, with a steep dip. Near the studied section, hydrothermally altered, goethitic Lower Cretaceous hyaloclastites, pillow basalts and Jurassic clastic sediments with ferruginous impregnation are exposed on the surface, and in a few drill cores metasomatized Lower Cretaceous goethitic volcanosediment were identified (Hetényi et al., 1976). Lower Cretaceous intrasediment submarine pillow-basaltic and hyaloclastitic sills occur in large thickness along the MZ tectonic zone suggesting that this tectonic zone was active during the Cretaceous (Jáger et al., 2012). Several subvolcanic dykes also occur in the Geresd Hills, which are likely to be Upper Cretaceous (Balla, 2009).

Materials and Methods

Thin sections were studied under a Nikon Eclipse E600 POL polarizing microscope at the University of Pécs, Hungary.

Scanning Electron microscopy with Electron Dispersive Spectroscopy (SEM-EDS) were performed using a Hitachi S-4800 instrument at the Zoltán Bay-Nanoscience Institute, Miskolc, Hungary and with a Jeol JSM-IT500HR instrument at the Szentágothai Research Center, Pécs, Hungary.

The filament-bearing samples were prepared for morphological analysis with SEM-BSE using 10 m/m% of HCl solution that was dropped to the surface of the thin sections for 20 seconds, than dipped into distilled water for 2 minutes and dried at room temperature before coating the samples with gold.

X-Ray Powder Diffraction (XRD) was used to determine mineral phases using a Rigaku MiniFlex 600 Bragg-Brentano diffractometer at the Szentágothai Research Centre, Pécs, Hungary, using CuKα radiation (λ = 1.54186 Å) and a proportional detector with a graphite monochromator in the reflected beam. The following analysis parameters were used: 40 kV, beam current of 15 mA, scan range of 3°–70° 2θ in continuous scan of 0.03° 2θ steps, with 1 s per step.

Raman spectroscopic analyses were performed at the University of Szeged, Hungary on a Thermo Scientific DXR Raman microscope equipped with a diode-pumped frequency-doubled Nd-YAG laser at 10mW maximum laser power. Samples were irradiated by laser light at a wavelength of 532.2 nm, with the laser beam focused using a 100× objective lens, resulting in a spot size of ~0.7 μm.

Trace element analyses were carried out at ALS Laboratory, Vancouver, Canada with an Agilent Technologies 725 ICP-OES and PerkinElmer ELAN® 9000 ICP-MS instrument. Only Au and Ag were measured with ICP-MS.

The total organic carbon content (TOC) of samples were measured using an Analytik Jena HT1300 solids module at the Szentágothai Research Centre, Pécs, Hungary. The organic carbon content of the solid samples was digested by oxidative combustion. During the measurement, the digestion temperature was 950 °C. Ceramic boats were used for sample introduction, and for blank sample. The solids module was connected with a non-dispersive infrared absorption (NDIR) detector. To determine the TOC concentration, 10 m/m% of HCl solution was used to remove the inorganic carbon content from the materials. The acid was added drop by drop to the samples, until no further reaction was observed. After this treatment the samples were placed in an exsiccator at 105 °C for at least three hours to dry, and the TOC content was measured afterward.

Nucleic acid isolation was performed at the Szentágothai Research Centre, Pécs, Hungary using an Omega Bio-Tek E.Z.N.A. Mag-Bind Soil DNA Kit according to the protocol with minor modifications. The quantity of the DNA was measured with a Qubit 2.0 fluorimeter. Prokaryotes 16S rRNA genes were amplified from the extracted DNA using 27f (AGAGTTTGATCMTGGCTCAG) and 519R (ATTACCGCGGCTGCTGG) primers. The PCR reaction was performed by DreamTaq DNA Polymerase (Thermo Scientific) in which the concentration of each primers concentration was 0,325 μM. Thermal cycling was performed using the Applied Biosystems® GeneAmp® PCR System 9700 and the PCR conditions were as follows: denaturation at 94°C for 30 s, annealing at 55°C for 30 s, and extension at 72°C for 30 sec with 30 min final extension step at 72°C. Amplification was carried out for 30 cycles. The amplified 16S rRNA genes were analysed on 1.5% agarose gel and the approximately 500 bp PCR products were excised then purified with QIAGEN Kit. Purified PCR products were cloned into pZT vector with Thermo Scientific InsTAclone PCR Cloning Kit. Plasmid insert DNA from clones containing ligated vector was amplified by using M13F (GTAAAACGACGGCCAG) and M13R (CAGGAAACAGCTATGAC) primers. The PCR products were directly sequenced by ABI PRISM 310 Genetic Analyzer with ABI Big-Dye Reaction Mix 3.1. Each sequences of clone were determined by sequencing both strands.

The sequences were corrected manually then submitted to similarity analysis by using gapped BLAST search algorithms with the GenBank/EMBL/DDBJ databases.

Fractal dimensions were measured on microscope images by a MATLAB routine (Frederic Moisy (2020) boxcount (https://www.mathworks.com/matlabcentral/fileexchange/13063 boxcount), MATLAB Central File Exchange. Retrieved May 17, 2020)

Directionality analysis was carried out whith the OrientationJ plugin of the ImageJ software package.

Results

1. Description of the hematitic carbonate dykes

A conspicuous red microcrystalline carbonaceous material fills fractures of a greenish-grey foliated metabasic rock body at the Goldgrund Valley (Fig. 1A, B). The red fill is flanked by white calcite veins towards the host metabasite (Fig. 1C), and locally contains fragments of the host rock with a "jigsaw-fit" breccia texture (Fig. 1D). The thickness of these veins varies from several mm up to 30 cm.

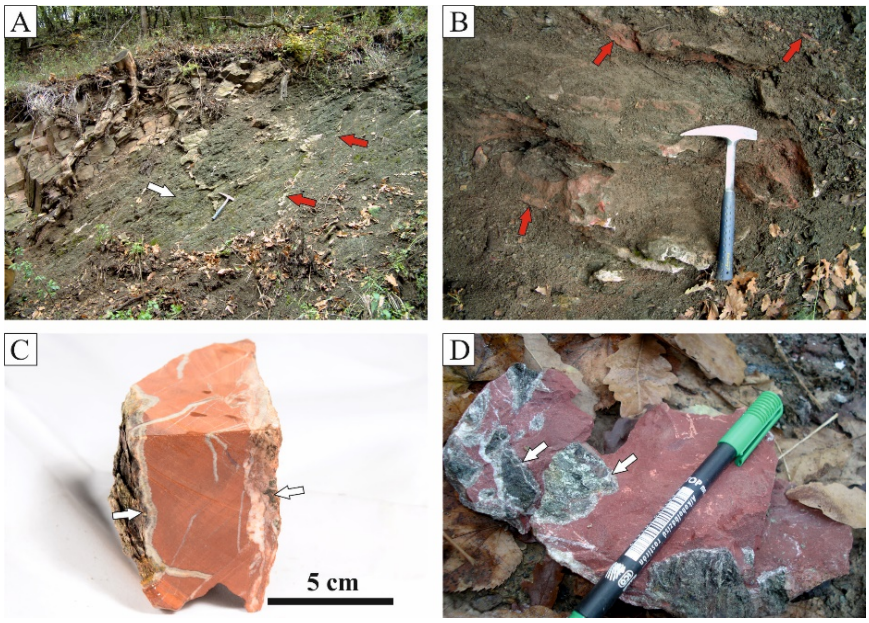

1. Figure *Characteristics of the studied outcrops and samples. (A) Mylonitic gneiss and foliated metabasite (white arrow) crosscut by injection dykes (red arrows). Rock hammer for scale. (B) Injection dyke system (red arrows) in the mylonitic, foliated metabasite. Rock hammer for scale. (C) Cut slab of a hematitic carbonate dyke sample. White arrows show the contact with the foliated host metabasic rock. (D) Field photo showing breccia clasts (white arrows) of the host metabasit enclosed in the calcite matrix of the hematitic carbonate dyke.*

The veins appear homogenous with the naked eye, but in thin section they show microlamination that is parallel with the surface of the fissure they fill (Fig. 2A). Microscopic and mineralogical analysis revealed that the red material in the fractures is finely to medium crystalline equant–blocky calcite mosaic spar (microspar to pseudospar *sensu* Bathurst, 1975) with dispersed hematite (Fig. 2B). The distribution of the crystal size in the calcite matrix is irregular and the intercrystalline boundaries are typically wavy (Fig. 2B). Hereinafter, we will refer to this hematitic carbonate material as hematitic carbonate dykes.

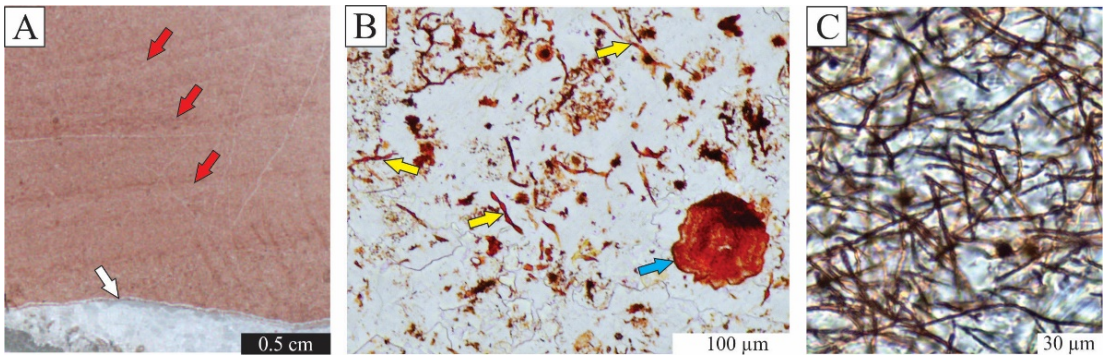

2. Figure Micro-scale characteristics of the hematitic carbonate dyke samples (A) Thin section image of a hematitic carbonate dyke sample showing microlaminations (red arrows). White arrow shows a calcite vein along the contact between the hematitic carbonate and metabasic host rock. Plane-polarized light. (B) Hematitic precipitates and filaments in fine to medium crystalline calcite matrix. Blue arrow points to a hematitic precipitate showing periodic, Liesegang-type pattern and yellow arrows point to helical filaments. Plane-polarized light. (C) Hematitic filaments (brown elongate particles) embedded in the fine to medium crystalline calcite matrix of the hematitic carbonate dykes. Plane-polarized light

2. Microfossils in the hematitic carbonate dykes

Well-preserved helical microfossils occur in the fracture filling hematitic carbonate dykes that crosscut the foliated metamorphic host rock (Fig. 2B, C). The helical morphology of the filaments strongly resembles the recent *Gallionella* and *Mariprofundus* spp. (Fig. 4; cf. Recent *Gallionella* and *Mariprofundus* in Emerson et al., 2010, their Fig. 3a, b). Locally in the micritic carbonate matrix, 1–2 mm sized clusters of helical-structured filaments can be observed with slightly preferred orientation (Fig. 3A). Some filaments have a strongly curled shape (Fig. 3E, G), or have a rod shape (Fig. 3H). These filamentous structures occur in a rock-forming quantity within the carbonate matrix.

The width of the helical microfossils varies between 1 and 5 µm and their lenghts reach up to about 100 µm. SEM and Raman observations revealed that these microfossils are built up of micron–submicron sized pseudohexagonal platy hematite, which are embedded in the helical matrix of the filaments (e.g. Fig. 3C). Other hematitic microfossils can also be distinguished in the hematitic carbonate dykes. These likely are pseudomorphs after foraminifer fossils. The size of these pseudomorphs do not exceed 90 µm. Based on the SEM-EDS and Raman investigations, these pseudomorphs are also composed of submicron–micron sized microcrystalline platy hematite. Some other particles show periodic Liesegang-type precipitation rings (Fig. 2B).

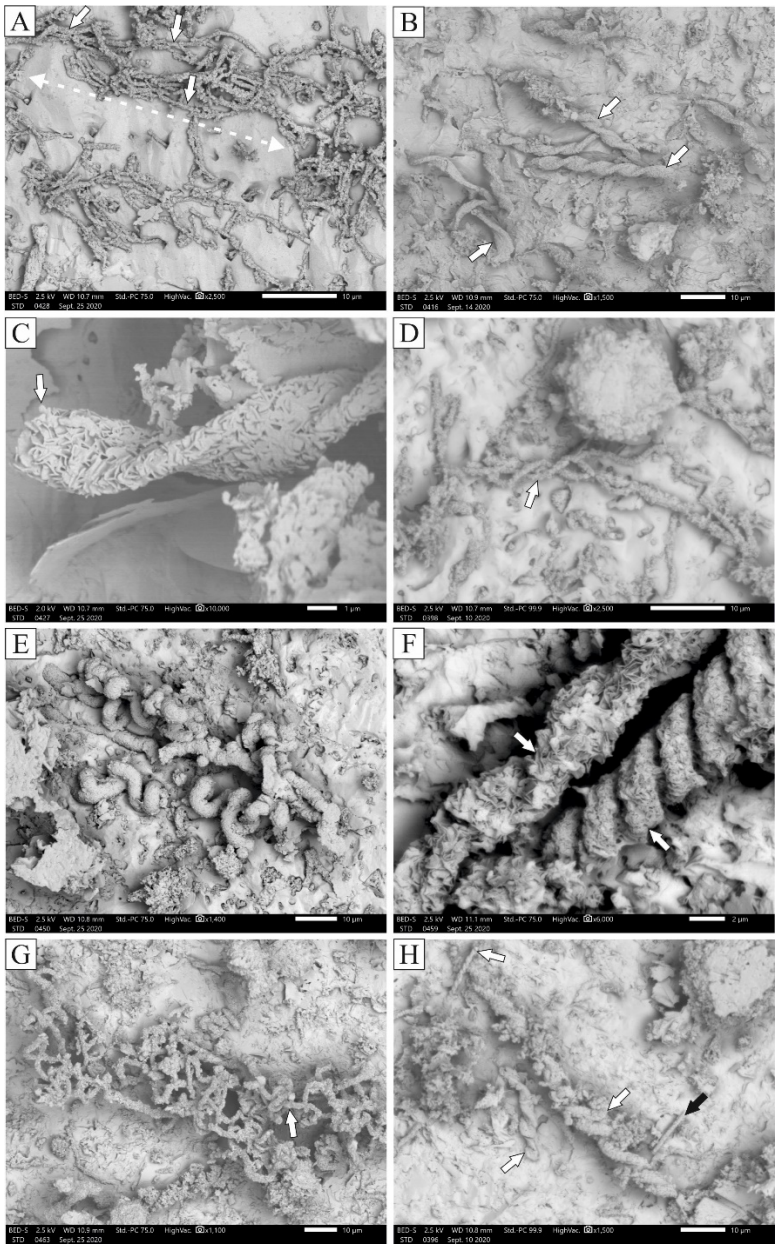

3. Figure SEM-BSE images showing mineralized FeOB stalk fossils (A) The hematitic filaments locally show slight preferred orientation (dashed white line), whereby the filaments appear arranged parallelly or subparallelly with one other (white arrows). (B) Helical structures with varying sizes and spiral density (white arrows). (C) A helical filament (white arrow) demonstrating that the filaments are comprised of micron-submicron sized pseudohexagonal platy hematite. (D) Unevenly twirled filamentous structure (white arrow). (E) Strongly curled filamentous structures (white arrow). (F) Filamentous structures with different curvature density. The more strongly rolled structure (red arrow) is characterized by finer crystal size of the hematitie plates than in the more weakly rolled structure (yellow arrow). (G) Curled filaments with chaotic arrangement. Note the constant widths of the structures (<5 µm). (H) Helical filaments of various sizes (width between 1 and 5 µm) and curvature density (white arrows). Helical structures are characteristic in these samples; however, less typically, straight, rod-like forms can also be found (black arrow).

3. Composition of the hematitic carbonate dykes

Several, mostly chalcophyle elements (As, Ba, Cd, Co, Cu, Mn, Mo, Pb, W) are enriched in the hematitic carbonates compared to the crustal average (cf., Rudnick and Gao, 2003). Sulphur was only detected in a few samples. SEM-EDS examination revealed that P, S and

Mg are only enriched in the helical filaments and Si is enriched both in the helical structures and in the foraminifer pseudomorphs, compared to the carbonate matrix. The Total Organic Carbon (TOC) content of two measured samples is 0.84 and 1.21 %.

4. *Analysis of bacterial DNA*

The amplified 16S rDNA using universal Eubacteria primers were sequenced to provide insight into the recent bacterial communities of the sample. The general BLAST search identified the presence of common bacteria species (e.g., *Bacillus*, *Bradyrhizobium*, *Lactococcus*, *Pseudomonas*) in 63% of the sequences. The second round of BLAST search focused on the *Gallionella* taxon; however, none of the sequences showed any significant similarity to the *Gallionella* sp.

5. *Fractal and directional analysis of the filamentous clusters*

Pictures were taken from 15 different locations in the thin sections containing the hematitic helical filamentous structures with the same resolution (300 dpi) and magnification (10x). The minimal fractal dimension that we measured is D_f = 1.876, the maximal is D_f = 1.934. The average of the fractal dimension is D_f = 1.900 with standard deviation of 0.017, so the relative standard deviation is less than 1%.

The directional distribution of the filamentous structures follows a normal distribution with a standard deviation of ~52° in the Gal13 and Gal14 samples (Diagram 1-2). Gal 1, 2, 3, 7, 8, 9, 10, 11 samples can be fitted with two Gaussian-curves and Gal 4, 5, 12, 15 samples can be fitted with three Gaussian curves. The distribution curves are fitted with (the sum of) one, two, or three Gaussian peaks with heights A_n, full-widths at half maximum w_n and centers xc_n.

$$y(x) = y_0 + \sum_{n=1}^{1,2,3} \frac{A_n}{w_n\sqrt{2\pi}} e^{\frac{-2(x-xc_n)^2}{w_n^2}}$$

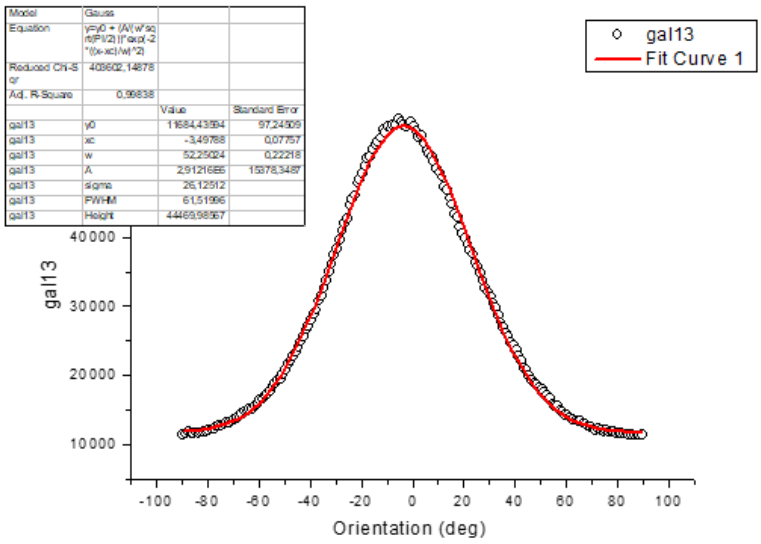

1. diagram. Directional distribution of the filamentous structures in the Gal13 sample

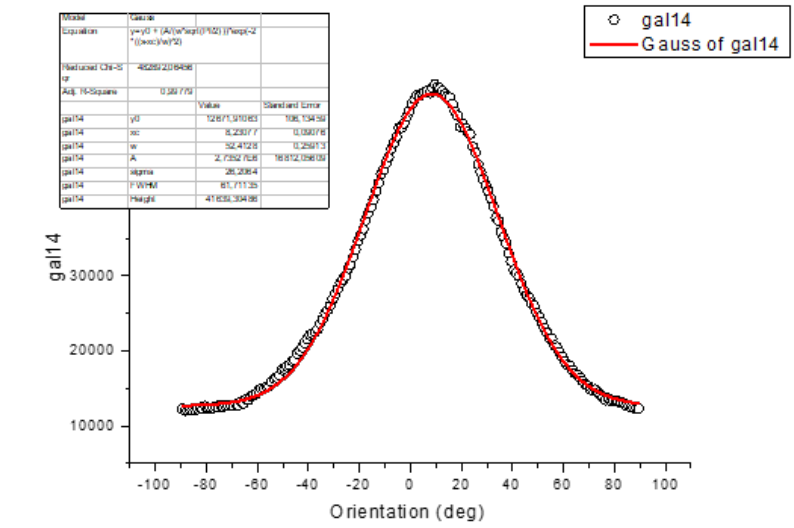

***2**. diagram. Directional distribution of the filamentous structures in the Gal14 sample*

Discussion

Formation of fissures and injection dykes

Important diagnostic features of the hematitic carbonate dykes in the Geresd Hills are the microlaminated texture of the microcrystalline material and the “jigsaw-fit” breccia texture of

the host metabasic rocks. These characteristics suggest the injection dyke origin of the hemtatitic carbonate dykes likely due to seismic shock induced fluid overpressure and hydraulic fracturing. Neptunian and injection dykes are the best known seismites and are usually associated with large active fault zones in an extensional stress field where they are typically used as syn-rift palaeostress indicators (Montenat et al., 1991; Beacom et al., 1999; Łuczyński 2001; Montenat et al., 2007; Kołodziej et al., 2010). The formation of injection dykes results from the hydrofracturing of a hard substrate and infilling of the fractures by overpressured, fluidized soft sediments (Flügel, 2004; Montenat et al., 2007; Kołodziej et al., 2010). Fissure networks formed nearby the fault zone commonly produce a "jigsaw-puzzle" pattern (Montenat et al., 2007). Neptunian dykes cause a large-scale diffusion of water and fine sediment that deeply penetrate the pores and voids of the basement rocks. These fluids may be subject to overpressure when seismic shocks occur in the fault zone, giving rise to injection dykes (Montenat et al., 2007). The presence of injection dykes in the metamorphic complex of Ófalu fits into the model of Dabi et al. (2011), who described a seven-stage fracturing history of the study area based on cross-cutting relationships. Their textural observations suggest that the first syntaxial calcite generation preserved long-standing remnant fracture porosity in the middle lines of the veins. The frequently co-occurring calcite selvage of the red calcite filled dykes suggest that their formation is related to the presence of the pre-existing calcite-filled veins. These veins likely retained some remnant fracture porosity along their middle lines at the time of the seismic event, acting as planes of weakness prone to reopening, and as conduits for the injection of lime mud, ultimately resulting in the formation of injection dykes. K/Ar data from the basaltic rocks of the Eastern Mecsek Mountains indicate that the main period of volcanic activity occurred between 135 and 110 Ma (Early Cretaceous) (Harangi and Árváné Sós, 1993), which is partly contemporaneous with the tectonic activity that affected the Carboniferous Mórágy Granite to the south (Balla et al., 2003). Early Cretaceous magmatic emplacent and related hydrothermal phenomena are described both from the study area and the Mórágy Granite to the south, e.g., gradual transition from thinner magmatic dykes to fractures filled with carbonate and limonitic material (Balla et al., 2009), altogether alluding to contemporaneous Cretaceous magmatic and tectonic activity in the study area. However, the Cretaceous tectonic activity is characterized mostly by strike slip faulting (Balla et al., 2009). Therefore, the partially filled calcite veins in the study area likely reopened in a strike slip tectonic regime, possibly in a pull apart segment.

Origin of the fissure filling material

The hematitic carbonate material in the injection dykes does not show any signs of metamorphic alteration, which is inferred from the well-preserved microlamination and the undeformed nature of the microfossils. This suggests that the tectonic event, which resulted in the opening of the fractures later filled with the hematitic carbonate, post-dates the Paleozoic metamorphism that had affected the Ófalu complex. The absence of terrigenous material and shallow marine fossils in the hematitic carbonate dykes suggests a pelagic origin of the lime mud that likely gushed into the fractures thus creating the injection dikes.

The current sparry calcite mosaic fabric of the carbonate material is likely the result of aggrading neomorphism during burial diagenesis. During aggrading neomorphism micron-sized $CaCO_3$ is replaced in situ by secondary calcite spar during a wet recrystallization (dissolution–re-precipitation) process along a fluid film resulting in crystal enlargement (Bathurst, 1975). Aggrading neomorphism is believed to be driven to increase the stability of the carbonate sediment since the smaller crystals of the original lime mud are more soluble, contain defects and impurities, and the original sediment may contain more soluble carbonate phases such as aragonite and high-magnesian calcite (Bathurst, 1975). The sulphur and total

organic carbon content of the samples together with higher concentrations of chalcophile elements (e.g., As, Cd, Co, Cu, Mo, Pb) suggest that the carbonate sediment may have deposited under anoxic or dysoxic conditions. However, post-depositional neomorphic alteration of the carbonate may have affected its chemical composition; thus, the measured elemental composition may not reflect the original depositional conditions. The Liesegang-bands in the hematitic particles likely resulted from the oxidation of iron sulphidic particles and the filamentous structures suggest that FeOB microbial mats might have been present in the sediment.

The habitat of Fe-oxidizing bacteria (FeOB)

Even though our DNA analysis did not confirm the presence of *Gallionella* in the samples, based on the helical morphology of the filaments we infer that these likely are remnants of fossils similar to the recent *Gallionella* and *Mariprofundus* spp. Lindahl (1993) showed that DNA cannot be preserved for more than a few thousands of years. Furthermore, Coolen and Overman (1998) inferred based on lake sediments that the DNA abundance of phototrophic microorganisms decreases by six orders of magnitudes over 11,000 years. Nevertheless Inagaki et al. (2005) proved that relatively dry, anoxic and clay-rich environments are favorable factors to preserve ancient DNA molecules for as long as 100 Ma. However, according to some scientists, DNA molecules in the Inagaki et al. (2005) samples are contaminations (Sinninghe Damsté and Coolen, 2006; Dong and Yu, 2007), hence the detected DNA in Inagaki et al. (2005) may not represent long-term DNA preservation. In our samples, the presence of recent bacterial communities also suggests that the DNA in the analysed samples derived from contamination and is not representative of the microbial communities at the time of formation of the hematitic carbonate material. Lipid biomarkers can be specific to microbial functional groups, and these components can be preserved in rocks longer than DNA molecules (Dong and Yu, 2007). Therefore, future analysis of biomarkers of samples from the Geresd Hills may provide insight into the origin of the microbial structures.

Nevertheless, due to the morphological similarity, we use the recent *Gallionella* and *Mariprofundus* spp. as an analogue to interpret the environment of microbial Fe oxidation in the Geresd Hills. The family Gallionellaceae has one known species, *Gallionella ferruginea* (Hallbeck et al., 1993; Hallbeck and Pedersen, 2005). Gallionellaceae have traditionally been associated with freshwater habitats, but studies have indicated that some members of this family are present in marine environments (Johannessen et al., 2017). The chemolithotrophic (use oxidation of inorganic compounds as a source of energy), neutrophilic (flourish in a neutral pH environment), aerotactic (movement toward oxygen), microaerophilic (flourish where oxygen level is low) betaproteobacterium *Gallionella ferruginea* occurs in sharply limited physico-chemical conditions characterized by a low redox potential; pH limits ranging from 6.0 to 7.6; temperature ranging up to 47 °C (with an optimal 8–20 °C temperatures), and a relatively low content of organic material (Ehrlich, 1990; Hallbeck and Pedersen 1990, 1995; Anderson et al., 2003; Hanert, 2006). For *Gallionella ferruginea*, both autotrophic (use carbon dioxide as their source of carbon) and mixotrophic (use a mix of different sources of energy and carbon, such as glucose, fructose, and sucrose) growth capabilities have been clearly shown (Hallbeck, 1991).

Based on our SEM-EDS examinations, P and S are enriched in the helical microfossils and Si is enriched both in helical and in foraminifer microfossils. Suzuki et al., (2011) found that Si and P represent the major inorganic components of *Gallionella ferruginea* fibers. Therefore, the the elevated P and Si contents in our samples may have resulted from the presence of *Gallionella*.

The also aerotactic zetaproteobacterium *Mariprofundus ferrooxydans* is an obligate chemolithotroph that oxidizes reduced iron from a variety of substrates at pH 5.5–7.2 and temperatures between 10–30 °C in the anoxic-oxic interfaces of marine environments (Singer et al., 2011; Krepski et al., 2013). Consequently, the most appropriate habitat for *Gallionella* and *Mariprofundus* is the anoxic-oxic mixing zone where spontaneous Fe oxidation is slow (Halbach et al., 2001). Besides Fe^{2+}, such a habitat often contains reduced sulpfur compounds (Halbach et al., 2001; Kato et al., 2012). Experiments of incubated marcasite and pyrite in the vicinity of a seafloor hydrothermal vent system and laboratory studies have provided evidence that autotrophic FeOB can grow from oxidation of the dissolution products of basalt glass and sulfide minerals (Edwards et al., 2003).

Primary evidence for FeOB in the deep sea is largely based on findings of flocculent ferrihydrite deposits (microbial mats up to 1 m thick) associated with relatively low-temperature, reduced iron enriched hydrothermal vents (10–100°C), which are most often associated with seamounts in the ocean (Emerson et al., 2010). In our case, previous volcanological, hydrogeological, geochemical and fluid inclusion studies (Dabi et al., 2011; Jáger et al., 2012; Dabi et al., 2013) fit the interpretation that the emplacement of Cretaceous submarine basaltic sills initiated a low-temperature discharge of reductive iron-rich fluids, which mixed with the oxygenated bottom waters and created a redox gradient favorable for the development of FeOB mats in the pelagic sediments that deposited on the seafloor.

Ferrihydrite – hematite reordering

Bacteriogenic iron oxyhydroxides, produced as a result of iron oxidation by FeOB are always poorly crystalline forms of ferrihydrite (Emerson et al., 2010). Ferrihydrite as a metastable mineral is known to be a precursor of more crystalline minerals such as hematite and goethite. At neutral pH, FeOB have been shown to increase the rate of iron oxidation by up to four orders of magnitude over the rate of strictly inorganic oxidation (Kasama and Murakami 2001; Neubauer et al., 2002). Even at 30 °C some iron oxidizers oxidize iron at 10-times higher rates than the corresponding abiotic rates (Vollrath et al., 2013), and they lower the degree of supersaturation required for ferrihydrite precipitation by behaving as geochemically reactive solids for heterogeneous surface nucleation (Stumm and Morgan 1996). Ferrihydrite is known to adsorb a wide range of inorganic and organic species (Benjamin and Leckie 1981; Cornell and Schwertmann, 2003) due to being a nanoporous material yielding a large surface area of several hundred square meters per gram (Hiemstra and Riemsdijk 2009). Elevated Cd, Co, Cu, Mn, Mo and Pb content of the investigated samples likely indicate such a high sorption capacity of the ferrihydrite. Elsewhere, high-resolution transmission electron microscopy (HRTEM) of biomineralization products of iron-oxidizing bacteria revealed an alternative coarsening mechanism in which adjacent 2- to 3-nanometer particles aggregate and rotate so their structures adopt parallel orientations in three dimensions (Banfield et al., 2000). Crystal growth is accomplished by eliminating water molecules at interfaces and forming iron-oxygen bonds leading to a coarser, polycrystalline mineral (Banfield et al., 2000). Since FeOB activity always produces poorly crystalline microporous ferrihydrite, the presence of the micron-submicron size hematite that comprise the helical filaments in the carbonate injection dykes at the Geresd Hills suggests the primary formation of bacteriogenic ferrihydrite, which later transformed into more stable goethite and subsequently into hematite Equations 1–3.

$$Fe^{2+} + 0.25\ O_2 + 2.5H_2O = Fe(OH)_{3(\text{ferrihydrite})} + 2H^+ \quad (1)$$

$$Fe(OH)_3 \rightarrow FeOOH_{(\text{goethite})} + H_2O \quad (2)$$

$$2FeOOH \rightarrow Fe_2O_{3(\text{hematite})} + H_2O \quad (3)$$

Filament orientation and fractal dimension analysis in aid of determining biogenicity

The preferred stalk orientation and subparallel texture of the filaments in our samples may be explained by preferential orientation due to cell movement toward oxygen. According to the experiments of Krepski et al. (2013), and the observations of Johannessen et al. (2017), *Mariprofundus ferrooxydans* and *Gallionella ferruginea* stalks displayed directional orientation, showing a bias in cell movement toward oxygen, indicating the cells are likely aerotactic. However, in several cases, unequivocal directionality could not be detected in our study; therefore, such origin for the preferred orientation is uncertain.

In many geologic settings chemical precipitations often exhibit self-organization or spontaneous ordering and have fractal geometries. Periodic precipitation has been studied to understand the mechanism of non-equilibrium pattern formation or periodic pattern formation which is basically explained by the Ostwald supersaturation theory (Toramaru et al., 2003), in which the coupling between diffusion and the reaction with supersaturation is essential. According to the experiments of Toramaru et al., (2003) at high gel concentrations, ordinary Liesegang band forms whereas at low gel concentrations, tree-like crystal aggregates similar to diffusion limited aggregation (DLA) develop in the entire system. Hopkinson et al., (1998) showed purely chemical self-organized ferric iron oxyhydroxide structures from the Trans-Atlantic Geotraverse (TAG) hydrothermal mound (Mid-Atlantic Ridge near 26°N, 45°W) that are very similar to bacterial structures, where ferric iron oxyhydroxide branching aggregates result from DLA growth mechanism catalysed by pyrite oxidation in siliceous gel. The fractal dimensions of the most common patterns range from D_f = 1.72 to D_f = 1.78, which are similar to the unique fractal dimension of the diffusion-limited aggregation algorithm D_f ~1.7 (Witten and Sander, 1983) and to the inorganic dendritic mineral DLA structures investigated by Chopard et al., (1991). Our analysed samples showed more complicated structures with significantly higher fractal dimension values between D_f ~ 1.87—1.93 compared to the purely inorganic filamentous and branching precipitates. The fractal dimension values together with morphological similarities to recent bacterial forms support the bacterial origin of the filamentous structures. Therefore, fractal dimension analysis may be a useful method to differentiate FeOB textures from dendritic mineralizations found in other rock samples at various locations and ages.

B. Cretaceous basalts that intruded into water-saturated sediments in the Eastern-Mecsek Mts. contain biomimetic miscrostructures and bacterial tunneling

Biogenic and biomimetic microstructures in hydrothermally altered basalt and interpillow sediment

A major challenge and a common subject of debates is how to distinguish bacterial structures and fossils from abiogenic alteration products and chemical precipitates (Hopkinson *et al.* 1998; García-Ruiz *et al.* 2002; Schopf *et al.* 2002; Livage, 2009; Brasier *et al.* 2002; McLoughlin *et al.* 2008b; McLoughlin *et al.* 2010; Schopf *et al.* 2010; Lepot *et al.* 2011; Rouillard et al., 2018; Johannessen *et al.* 2019; McMahon 2019).

Tubular and filamentous microstructures, Liesegang bands and stromatolite-like structures were observed at *Pusztakisfalu* and in *Jánosi-puszta* sections. These peculiar

structures may form as a result of either biogenic or abiogenic processes and will be discussed here.

Results

At Pusztakisfalu, strongly goethitic and peperitic limestone and fluidal breccia can be found at the upper contact of a basaltic sill. Elongated protrusions of thin smectitic/celadonitic and goethitic material appear along the upper hyaloclastitic rim of the sill (Fig. 4a-f). The volcanic glass altered into X-ray amorphous palagonite (microcrystalline precursor of smectite) and smectite/celadonite, goethite identified by XRD examinations. Goethite appears as single precipitation or in the mid-line of smectitic-celadonitic protrusions (Fig. 4f). This formation is typical where hyaloclastite has a hydrothermal overprint along fractures. Pure celadonitic filaments mostly occur in thick cracks in basaltic rocks. Quartz and locally microcrystalline hematite are associated with the celadonitic filaments. The size of the palagonitic and smectitic protrusion structures ranges from 5 μm to mm-sized. Goethitic filamentous inclusions in the palagonite also have a wide size range, where the thinnest filaments and elongated structures are about 1 μm wide. Branching and dendritic structures are common, where acicular goethite crystals can be seen along the filaments. Spherical formations, which are made up of rows of ball-shaped goethite, also typically occur in 2 μm thickness. Along the goethitic filaments, an X-ray amorphous green silicate mineral occurs, but in some places – as identified by XRD examinations – smectite or celadonite-1M coats the thin goethite filaments with tiny crystals (Fig. 4g). Concentric and rhythmic μm-wide Liesegang-type precipitations of X-ray amorphous silicate and goethite are also typical (Fig. 4h).

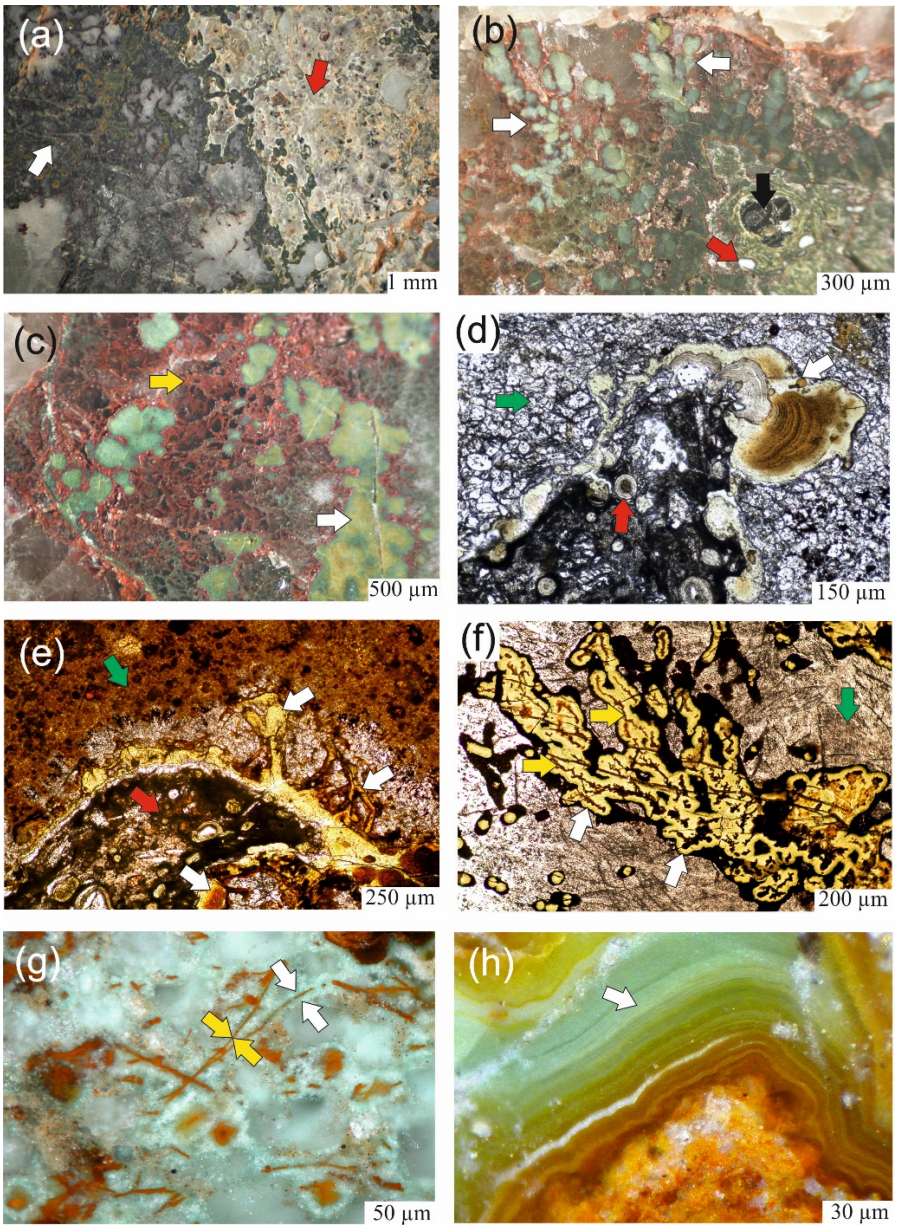

*4. Figure Chemical self-organized structures in the intrusive hyaloclastite, Pusztakisfalu, Mecsek Mts. (**a**) Transition of vesicular hyaloclastite (red arrow) into smectitic-goethitic dendrites (white arrow) in recrystallized carbonate. (**b**) Transition of vesicular hyaloclastite (red arrow) protrusions with ilmenite (black arrow) into smectitic-goethitic structures (white arrow) in recrystallized carbonate. (**c**) Alteration of basaltic glass into dendritic goethite (yellow arrow) and smectite (white arrow) in carbonate. (**d**) Amorphous palagonite "chemical stromatolite" structures (white arrow) developed along the interface of the host limestone (green arrow) and vesicular intrusive hyaloclastite (red arrow). (**e**) Protrusions of amorphous palagonite (white arrow) developed from the rim of the intrusive hyaloclastite (red arrow) and penetrated into the host sedimentary carbonate (green arrow). (**f**) In the midline of the palagonitic structures, goethitic precipitations can typically be found (yellow arrow). (**g**) Celadonite (white arrow) coating along goethite filaments (yellow arrow) in recrystallized carbonate. (**h**) Goethitic amorphous silicate (white arrow) with Liesegang-structure.*

Filamentous, dendritic and concentric textures also typically occur in peperites that are situated between intrusive pillows or appear as inclusions in hyaloclastite. Filamentous, "stromatolite-like" and dendritic smectitic alteration structures typically occur in the palagonitized parts of the hyaloclastite. These structures developed at the contact between the

hyaloclastite and the limestone. The alteration structures vary considerably in size from about 30 µm to a few mm (Fig. 5a-b).

In many parts of the hydrothermally altered intrusive hyaloclastite samples, along fractures of the rock, several microtubular structures occur in the altered volcanic glass with a uniform width of 1.5 µm and up to 200 µm in length, without intersecting one other. The microtubules are rarely bifurcate and curvy. These structures with constant and nearly bacterial cell-size diameter highly resemble bacterial tunneling structures (Fig. 5c). Fibrous goethite occurs along the microtubule walls in some parts of the altered hyaloclastite (Fig. 5d).

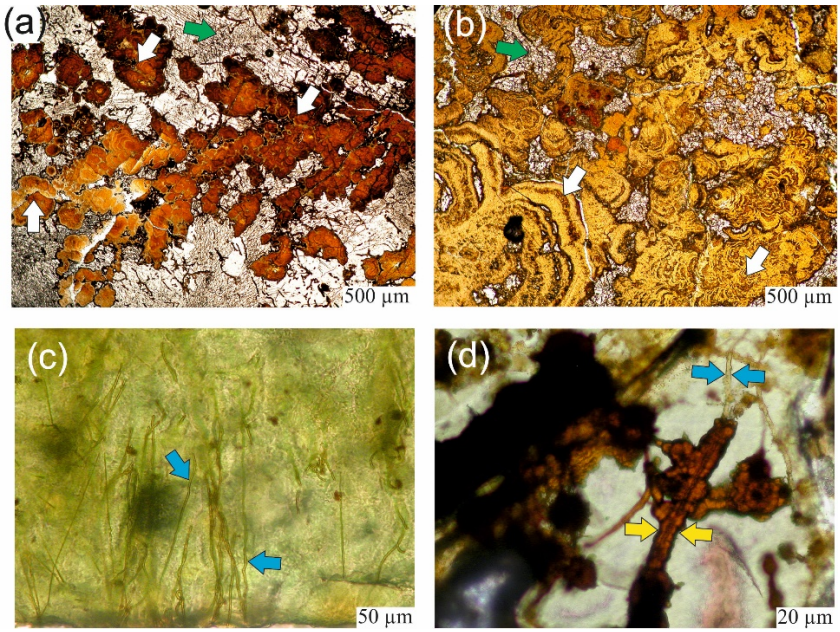

***5**. Figure "Chemical stromatolites" and bacterial-like bioalteration structures in the intrusive hyaloclastite, Pusztakisfalu, Mecsek Mts. (**a**) Smectite structures ("Chemical-stromatolite") (white arrow) in recrystallized carbonate (green arrow) from the glassy rim of the intrusive hyaloclastite. (**b**) Smectitic "chemical stromatolite" from the intrusive hyaloclastite. (**c**) Bacterial-like bioalteration structures with constant width (blue arrow) in the palagonitized volcanic glass of the intrusive hyaloclastite. (**d**) Fibrous goethite precipitations (yellow arrow) along microtubules (blue arrow) in the palagonitized intrusive hyaloclastite.*

In an other site of the Easter-Mecsek Mts., in the valley of the *Jánosi-puszta* section an approx. 240 m thick volcano-sedimentary sequence crops out. Unusual, geothitic, smectitic filamentous alteration structures of crustacean coprolites can be observed in the hydrothermally altered interpillow limestone. The diameter of the filaments ranges widely between 1 µm to several µm. Slightly elevated *S, Cl* and *P* content was measured in the filaments of the hydrothermally altered crustacean coprolite sample (Fig. 6a-c).

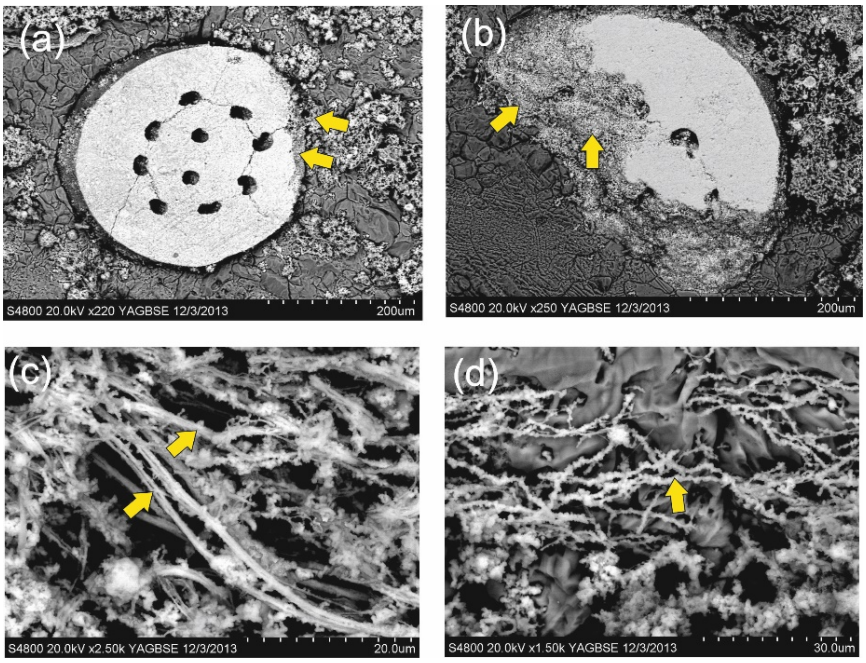

*6. Figure. Filamentous, biomorphic alteration textures of crustacean coprolites in the Lower Cretaceous interpillow limestone of Jánosi-puszta, Mecsek Mts. (**a-d**) Decapod crustacean coprolite with smectitic-goethitic filamentous alteration features (yellow arrow) from Jánosi-puszta*

Discussion

Bioalteration of volcanic glass

The presence of numerous, uniformly 1.5 µm wide tubular microstructures that penetrate to a depth of 200 µm without intersecting one another is typical in the *Pusztakisfalu* intrusive hyaloclastite along fractures in the rock (Fig. 6c, d). Such characteristics are consistent with formation by microbially enhanced glass dissolution (Staudigel *et al.* 2008*a*, *b*) and may be explained by the activity of Fe-oxidizers in the glassy material of the basaltic sills. These Fe-oxidisers likely contributed to the oxidation of reduced iron in the basalt and the released ferrihydrite associated with the *Pusztakisfalu* iron ore. Laboratory studies by others, which provided evidence that autotrophic Fe-oxidizing bacteria can grow from the dissolution products of basalt glass, support this hypothesis (Edwards *et al.* 2003; Thorseth *et al.* 2003).

Abiotic self-organization processes resulting in biomimetic microstructures

Abiotic oxidation and hydrothermal processes can create biomorphic formations such as stromatolite-like structures, coccoidal or filamentous microstructures, even in the size range of bacterial cells. Such forms and structures can also be obtained via chemical synthesis from purely inorganic precursors (García-Ruiz *et al.* 2002; Brasier *et al.* 2002; Livage 2009; Rouillard *et al.* 2018; McMahon 2019), like amorphous palagonite gels or clay-like materials that formed upon hydrothermal alteration of basaltic glass (Stroncik and Schmincke, 2002). Chemical precipitations often exhibit self-organization or spontaneous ordering. Periodic precipitation, otherwise known as Liesegang band, has been studied to understand the mechanism of non-equilibrium pattern formation or periodic pattern formation, which are explained by the Ostwald supersaturation theory (Toramaru *et al.* 2003). Such Liesegang

bands can be see in Fig. 4h, and are interpreted as a result of palagonitization and hydrothermal alteration of the basaltic glass. According to the experiments of Toramaru *et al.* (2003), ordinary Liesegang band forms at high gel concentrations, whereas tree-like crystal aggregates, similar to diffusion limited aggregation (DLA) develop in the entire system at low gel concentrations.

Hopkinson *et al.* (1998) showed purely chemically self-organized structures from the TAG (Trans-Atlantic Geotraverse) hydrothermal mound that are very similar to bacterial structures, where ferric iron oxyhydroxide branching aggregates result from diffusion limited aggregation (DLA) growth mechanism catalyzed by pyrite oxidation in siliceous gel. Periodic precipitation often creates stromatolite-like structures or "chemical stromatolites" (McLoughlin *et al.* 2008*b*).

Chemical gardens or silica gardens are other examples for self-organizing systems that result in hollow fibers and filaments that may resemble biological formations. During the formation of these structures, the precipitation of oxides or hydroxides from aqueous solutions of metal salts is mainly governed by the pH of the solution (Livage 2009). Most recently, McMahon (2019) synthesized hollow, minimum 1.8 μm-wide Fe-(oxyhydr)oxide biomorphic tubes with amorphous Fe-Si phases by "chemical gardening." In the case of the *Pusztakisfalu* section where slow diffusion of low temperature hydrothermal fluids likely occurred (along the fissures of intrusive pillows and the cracks of intrusive hyaloclastites), basaltic glass alteration into amorphous palagonite and smectite show periodic precipitation patterns and chemical garden-like structures. The hydrothermal alteration of the basaltic material into these fibrous, dendritic and periodic structures are clearly traceable in the calcite matrix (Fig. 5, Fig. 6a-b), even without morphometric investigations suggested by Rouillard *et al.* (2018). Such structures can be considered as a hydrothermal alteration product of the basaltic glass according to Dekov *et al.* (2007), who found that smectite can also form via the interaction of hydrothermal silica and iron oxyhydroxides which are possible constituents of the chemical garden filaments.

Besides the hydrothermal alteration structures of the basaltic hyaloclastite, hydrothermal decomposition of amorphous crustacean coprolites into smectite also resulted in similar filamentous and bacterial like structures (Fig. 6c-d), where the large surface area of the parallelly formed smectitic filaments likely played a role in the passive sorption of iron hydroxide released from the hydrothermally altered hyaloclastite and pillow-rims.

CONCLUSIONS

Based on our ancient bacterial and biomimetic structure foundings, it can be concluded that comprehensive studies involving multidisciplinary researches cannot be omitted. We described several natural processes which resulted in filamentous, dendritic and periodic biomimetic microstructures (e.g hydrothermal alteration of crustacean decapod's coprolites, hydrothermal alteration of volcanic glass). Furthermore we presented traces of an ancient Fe-oxidizing bacterial activity which created also filamentous microstructures from geological samples of the Eastern-Mecsek Mts. and from the Geresd-Hills. Based on our investigations,

we can say that the mathematical analysis of microstructures having unknown origin can help to identify ancient bacterial structures and ancient cell movements (based on the stalk directionality) of bacteria and can be effective for the differentiations of purely abiotic precipitations from organic structures. The multidisciplinary approach cannot be neglected with detailed geological, mineralogical, geochemical and biological analysis of the questionable system hosting these structures.

Morphological and directional analysis of the helical stalks of the FeOB suggest that the sub-parallel preferred orientation of the filaments may represent aerotactic cell movement toward oxygen. The higher mean value of the fractal dimensions ($D_f \sim 1.9$) measured in the microbial structures compared to the common fractal dimensions of similar but inorganic Fe-oxyhydroxide DLA-structures ($D_f \sim 1.7$) suggest that fractal dimension analysis may be a useful method to differentiate organic structures, such as FeOB mats, from similar inorganic precipitation structures. Since FeOB activity always produces poorly crystalline microporous ferrihydrite, the presence of the micron-submicron size hematite that comprise the helical filaments suggests the primary formation of bacteriogenic ferrihydrite, which later transformed into more stable goethite and subsequently into microcrystalline hematite.

In some cases, hydrothermal alteration of organic material and volcanic glass can be traced and the chemical origin of the bacterial-like structure is clear.

Based on our consultations with professor Tamás Vicsek, the next step in the development of mathematical methods for the differentiations of microstructures with different origin would be the application of the wavelet transforms.

In several studies, bacterial involvement in giant ore formations have been suggested, but the obvious morphological features identified in our studied rocks are missing from some of those publications. Because there is no complete consensus on the genetics of some of these ore formations, it is expected that the results of our mathematical modelling may help to address this issue and serve as a starting point for further researches.

References

Anderson, C. R., and Pedersen, K., 2003. In situ growth of Gallionella biofilms and partitionating of lanthanids and actinides between biological material and ferric oxyhydroxides. Geobiology, 1, 169–178.

Balla, Z., Császár, G., Gulácsi, Z., Gyalog, L., Kaiser, M., Király, E., Koloszár, L., Koroknai, B., Magyari, Á., Maros, Gy., Marsi, I., Molnár, P., Rotárné, Á., Szalkai, Gy Tóth. 2009. Geology of the North-eastern Part of the Mórágy Block. Geological Institute of Hungary, Budapest.

Banfield, J.F., Welch, S.A., Zhang, H., Ebert, T.T., Penn, R.L., 2000. Aggregation-based crystal growth and microstructure development in natural iron oxyhydroxide biomineralization products. Science. 289, 751–754.

Bathurst, R.G.C., 1975. Carbonate sediments and their diagenesis. Developments in Sedimentology 12, Second Enlarged Edition, Elsevier Scientific Publishing Company, Netherlands, 657 p.

Beacom, L.E. Anderson, T.B., Holdsworth, R.E 1999. Using basement-hosted clastic dykes as syn-rifting palaeostress indicators: an example from the basal Stoer Group, northwest Scotland Geol. Mag. 136, 301–310.

Benjamin, M.M. and Leckie, J. O., 1981. Multiple-site adsorption of Cd, Cu, Zn and Pb on amorphous iron oxyhydroxide. J. Colloid Interface Sci. 79, 209–221.

Boyce, A. J., Little, C. T. S., & Russell, M. J., 2003. A new fossil vent biota in the Ballynoe barite deposit, Silvermines, Ireland: Evidence for intracratonic sea-floor hydrothermal activity about 352 Ma. Economic Geology, 98, 649–656. https ://doi.org/10.2113/98.3.649

Brasier, M.D., Green, O.R., Jephcoat, A.P., Kleppe, A.K., Van Kranendonk, M.J., Lindsay, J.F., Steele, A., Grassineau, N.V., 2002. Questioning the evidence for Earth's oldest fossils, *Nature*, 416, 76–81.

Chan, C.S., Fakra, S.C, Emerson, D., Fleming, E.J., Edwards, K. J., 2011. Lithotrophic iron-oxidizing bacteria produce organic stalks to control mineral growth: implications for biosignature formation. The ISME Journal. 5, 717–727.

Chopard, B., Herrmann, H.J., Vicsek, T., 1991. Structure and growth mechanism of mineral dendrites. Nature, 353, 409–412.

Coolen, Marco J. L., Overmann, J. 1998. Analysis of Subfossil Molecular Remains of Purple Sulfur Bacteria in a Lake Sediment. Applied and Environmental Microbiology. 64, 4513–4521.

Cronan, D.S., Varnavas, S.P., Hodkinson, R., 2000. Hydrothermal mineralizing processes and associated sedimentation in the Santorini hydrothermal embayments. Marine Georesources and Geotechnology, 18, 77–118.

Cornell, R.M. and Schwertmann, U., 2003. The Iron Oxides. 2nd edn. Weinheim: Wiley-VCH, 664 pp.

Dabi, G., Siklósy, Z., Schubert, F., Bajnóczi, B., M. Tóth, T. 2011. The relevance of vein texture in understanding the past hydraulic behaviour of a crystalline rock mass: reconstruction of the palaeohydrology of the Mecsekalja Zone, South Hungary. Geofluids, 11, 309–327.

Dabi, G., Bajnóczi, B., Schubert, F., M. Tóth, T. 2013. The origin and role of a calcite-filled microcrack generation in a metamorphic crystalline complex: The characterization of a fossilised seismic permeability system. Tectonophysics. 608, 792–803.

Dekov, V. M, Kamenov, G.D., Stummeyer, J., Thiry, M., Savelli, C., Shanks, W. C., Fortin, D., Kuzmann, E., Vértes, A., 2007. Hydrothermal nontronite formation at Eolo seamount (Aeolian volcanic arc, Tyrrhenian Sea). *Chem. Geol*. **245**, 103–119. https://doi.org/10.1016/j.chemgeo.2007.08.006

Dong, H., Yu, B. 2007. Geomicrobiological processes in extreme environments. Episodes. 30, 3. 202–216.

Edwards, K.J., McCollom, T.M., Konishi, H. and Buseck, P.R., 2003. Seafloor bio-alteration of sulfide minerals: Results from in-situ incubation studies. Geochimica et Cosmochimica Acta. 67, (15), 2843–2856.

Edwards, K. J., Glazer, B. T., Rouxel, O. J., Bach, W., Emerson, D., Davis, R. E., Toner, B. M., Chan, C. S., Tebo, B. M., Staudigel, H., Moyer, C. L., 2011. Ultra-diffuse Hydrothermal Venting Supports Fe-oxidizing Bacteria and Massive Umber Deposition at 5000m off Hawaii. ISME Journal. 5, 1748–1758.

Edwards, C.T., Pufahl, P.K., Hiatt, E.E., Kyser, T.K., 2012. Paleoenvironmental and taphonomic controls on the occurrence of Paleoproterozoic microbial communities in the 1.88 Ga Ferriman Group, Labrador Trough, Canada. Precambrian Res. 212, 91–106.

Ehrlich, H.L. 1990. Geomicrobiology (2nd ed.). Marcel Dekker, New York, 646 pp.

Emerson, D., C. L. Moyer. 2002. Neutrophilic Fe-Oxidizing Bacteria are abundant at the Loihi Seamount hydrothermal vents and play a major role in Fe oxide deposition. App. Environ. Microbiol. 68, 3085–3093.

Emerson, D., Fleming, E.J., McBeth, J.M. 2010. Iron-oxidizing bacteria: an environmental and genomic perspective. Annu. Rev. Microbiol. 64, 561–583.

Flügel, E., 2004. Microfacies of Carbonate Rocks: Analysis, Interpretation and Application. Springer Verlag, Berlin, 976 pp.

García-Ruiz, J.M., Carnerup, A., Christy, A.G., Welham, N.J., Hyde, S.T., 2002. Morphology: an ambiguous indicator of biogenicity, *Astrobiology*, 2, 353–370.

Haas, J. & Péró, Cs., 2004. Mesozoic evolution of the Tisza Mega-unit. International Journal of Earth Sciences. 93, 297–313.

Halbach, M., Koschinsky, A., Halbach, P., 2001. Report on the discovery of Gallionella ferruginea from an active hydrothermal field in the deep sea. Inter–Ridge News. 10, 18–20.

Hallbeck, L., and K. Pedersen. 1990. Culture parameters regulating stalk formation and growth rate of Gallionella ferruginea. J. Gen. Microbiol. 136, 1675–1680.

Hallbeck, L., and Pedersen, K., 1995. Benefits associated with the stalk of Gallionella ferruginea, evaluated by comparison of a stalk-forming and a non-stalk-forming strain and biofilm studies in situ, Microbial Ecology. 30, 257–268.

Hallbeck, L., Stahl, F. and Pedersen K., 1993. Phylogeny and phenotypic characterization of the stalk-forming and ironoxidizing bacterium Gallionella ferruginea. J. Gen. Microbiol. 139, 1531–1535.

Hallbeck, L. E., and Pedersen, K., 2005. Genus I. Gallionella Ehrenberg 1838 166AL, In Brenner, D. J., Krieg, N. R., and Staley, J. T. (eds.), Bergey's Manual of Systematic Bacteriology. The Proteobacteria. Part C. The Alpha-, Beta-, Delta and Epsilonproteobacteria. New York: Springer. 2, 880–886.

Hanert, H.H., 2002. Bacterial and chemical iron oxide deposition in a shallow bay on Palaea Kameni, Santorini, Greece: microscopy, electron probe microanalysis, and photometry of in situ experiments. Geomicrobiology Journal. 19, 317–342.

Hanert, H.H. 2006. The genus Gallionella. In: Dworkin MM, Schleifer K-H, Rosenberg E, Falkow S, editors. The Prokaryotes. New York: Springer. 7, 990–995. https ://doi.org/10.1007/0-387-30747-8_46

Hetényi, R., Földi, M., Hámor, G., Nagy, I., Bilik, I., Jantsky, B., 1976. Magyarázó a Mecsek hegység földtani térképéhez, 10 000-es sorozat, Ófalu. MÁFI-Budapest (In Hungarian).

Hiemstra, T and Riemsdijk, Van W. H., 2009. A surface structural model for ferrihydrite I: Sites related to primary charge, molar mass, and mass density Geochimica et Cosmochimica Acta. 73, 4423–4436.

Holm, N.G. 1987. Biogenic influences on the geochemistry of certain ferruginous sediments of hydrothermal origin. Chem. Geol. 63, 45–57

Hopkinson, L. Roberts, S. Herrington, R. and Wilkinson, J. 1998. Self-organization of submarine hydrothermal siliceous deposits: Evidence from the TAG hydrothermal mound, 26°N Mid-Atlantic Ridge. Geology. 26, 347–350.

Hrischeva, E., Scott, S.D., 2007. Geochemistry and morphology of metalliferous sediments and oxyhydroxides from the Endeavour segment, Juan de Fuca Ridge. Geochimica et Cosmochimica Acta. 71, 3476–3497.

Inagaki, F., Okada, H., Tsapin, A.I., and Nealson, K.H., 2005. The Paleome: a sedimentary genetic record of past microbial communities. Astrobiology. 5, 41–153.

Jáger, V., Molnár, F., Buchs, D., Koděra, P., 2012. The connection between iron ore formations and "mud-shrimp" colonizations around sunken wood debris and hydrothermal sediments in a lower cretaceous continental rift basin, Mecsek Mts., Hungary. Earth Sci. Rev. 114, 250–278.

Johannessen, K. C., Vander Roost, J., Dahle, H., Dundas, S. H., Pedersen, R. B., & Thorseth, I. H., 2017. Environmental controls on biomineralization and Fe-mound formation in a low-temperature hydrothermal system at the Jan Mayen Vent Fields. Geochimica Et CosmochimicaActa. 202, 101–123. https ://doi.org/10.1016/j.gca.2016.12.016

Kappler, A., Pasquero, C., Konhauser, K.O., Newman, D.K. 2005. Deposition of banded iron formations by anoxygenic phototrophic Fe2+-oxidizing bacteria. Geology. 33, 865–868.

Kasama, T. and Murakami, T., 2001. The effect of microorganisms on Fe precipitation rates at neutral pH. Chem. Geol. 180, 117–128.

Kato, S., Kikuchi, S., Kashiwabara, T., Takahashi, Y., Suzuki, K., Itoh, T., Ohkuma,M., Yamagish, A. 2012. Prokaryotic abundance and community composition in a freshwater iron-rich microbial mat at circumneutral pH. Geomicrobiology Journal. 29, (10), 896–905.

Kennedy, C. B., Scott, S. D. and Ferris, F. G., 2003. Characterization of bacteriogenic iron oxide deposits from axial volcano, Juan de Fuca Ridge, Northeast Pacific Ocean. Geomicrobiol. J. 20, 199.

Konhauser, K.O., 1998. Diversity of bacterial iron mineralization. Earth-Science Reviews. 43, 91–121.

Krepski, S. T., Emerson, D., Hredzak-Showalter, P. L., Luther, G. W., & Chan, C. S., 2013. Morphology of biogenic iron oxides records microbial physiology and environmental conditions: Toward interpreting iron microfossils. Geobiology, 11, 457–471.

Lepot, K., Benzerara, K., Philippot, P., 2011. Biogenic versus metamorphic origins of diverse microtubes in 2.7 Gyr old volcanic ashes: Multi-scale investigations. *Earth and Planetary Science Letters*, **312**, 37–47.

Li, J., Su, L., Wang, F., Yang, J., Gu, L., Sun, M., Li, Q., Zhou, H., Fang, J., 2020. Elucidating the biomineralization of low-temperature hydrothermal precipitates with varying Fe, Si contents: Indication from ultrastructure and microbiological analyses. Deep-Sea Research Part I. Oceanographic Research Papers 157, DOI: 10.1016/j.dsr.2019.103208.

Lin, Y., Tang,D., Shi,X., Zhou, X., Huang, K., 2019. Shallow-marine ironstones formed by microaerophilic iron-oxidizing bacteria in terminal Paleoproterozoic. Gondwana Research. 76, 1–18.

Lindahl, T. 1993 Recovery of antediluvian DNA. Nature. 365, 700.

Little, C.T.S., Glynn, Sarah E.J., Mills, A.R., 2004. Four-hundred-and-ninety-million-year record of bacteriogenic iron oxide precipitation at sea-floor hydrothermal vents. Geomicrobiology Journal. 21, 415–429.

Livage, J. 2009. Chemical synthesis of biomimetic forms. *C. R. Palevol*, 8, 629–636.

Łuczyński, P. 2001. Development history of Middle Jurassic neptunian dykes in the High-Tatric series, Tatra Mountains, Poland. Acta Geologica Polonica. 51 (3), 237–252.

McLoughlin, N., Wilson, L. A., Brasier, M. D., 2008b. Growth of synthetic stromatolites and wrinkle structures in the absence of microbes – implications for the early fossil record. *Geobiology*, **6**, 95–105.

McLoughlin, N., Staudigel, H., Furnes, H., Eickmann, B., Ivarsson, M., 2010. Mechanisms of microtunneling in rock substrates: distinguishing endolithic biosignatures from abiotic microtunnels. *Geobiology*, **8**, 245–255.

McMahon, S., 2019. Earth's earliest and deepest purported fossils may be iron-mineralized chemical gardens. *Proc. R. Soc. B,* **286**, 20192410*,* http://dx.doi.org/10.1098/rspb.2019.2410

M. Tóth, T., Kovács, G., Schubert, F., Dályai, V., 2005. Origin and deformation history of the Ófalu migmatite. Bull. Hung. Geol. Soc. 135, 331–352.

Montenat, C., Barier, P. & Ott d'Estevou, P., 1991. Some aspects of the recent tectonics in the Strait of Messina, Italy. Tectonophysics. 194, 227–244.

Montenat, C., Barrier, P., Ott d'Estevou, P. & Hibsch, C., 2007. Seismites: An attempt at critical analysis and classification. Sedimentary Geology. 196, 5–30.

Neubauer, S.C., Emerson, D., and Megonigal, J.P., 2002, Life at the energetic edge: Kinetics of circumneutral iron oxidation by lithotrophic iron-oxidizing bacteria isolated from the wetland-plant rhizosphere. Applied and Environmental Microbiology. 68, 3988–3995.

Rose, A. W. and Bianchi-Mosquera G.C., 1993. Adsorption of Cu, Pb, Zn, Co, Ni, and Ag on Goethite and Hematite. A Control on Metal Mobilization from Red Beds into Stratiform Copper Deposits. Economic Geology, 88, 1226–1236.

Rouillard, J., García-Ruiz, J.M., Gong, J., Van Zuilen, M.A., 2018. A morphogram for silica-witherite biomorphs and its application to microfossil identification in the early Earth rock record. *Geobiology*, **16**, 279–296, https://doi.org/10.1111/gbi.12278

Rubin-Blum, M., Gilad, A., Tsadok, R., Shemesh, E., Austin, J.J.A., Coleman, D.F., Goodman-Tchernov, B.N., Ben-Avram, Z., Tchernov, D., 2014. First Evidence for the Presence of Iron Oxidizing Zetaproteobacteria at the Levantine Continental Margins. PLoS ONE 9(3):e91456. https://doi.org/10.1371/journal.pone.0091456.

Rudnick, R.L. and Gao, S. (2003). Composition of the continental crust. Treatise on Geochemistry, vol. 3, The Crust, Elsevier, pp. 1–64.

Schopf, J.W., Kudryavtsev, A.B., Agresti, D.G., Wdowiak, T.J., Czaja, A.D., 2002. Laser-Raman imagery of Earth's earliest fossils, *Nature*, 416, 73–76.

Schopf, J.W., Kudryavtsev, A.B., Sugitani, K.d, Walter, M.R., 2010. Precambrian microbe-like pseudofossils: A promising solution to the problem. *Precambrian Research*, **179**, 191–205.

Singer E., Emerson D., Webb E. A., Barco R. A., Kuenen J. G., Nelson W. C., Chan C. S., Comolli L. R., Ferriera S., Johnson J., Heidelberg J. F. and Edwards K. K., 2011. Mariprofundus ferrooxydans PV-1 the First Genome of a Marine Fe(II) Oxidizing Zetaproteobacterium. PLoS ONE 6, e25386.

Sinninghe Damsté, S.J., Coolen, M.J.L. 2006. Fossil DNA in Cretaceous black shales: myth or reality. Astrobiology. 6, 299–302.

Staudigel, H., Furnes, H., McLoughlin, N., Banerjee, N.R., Connell, L.B.,Templeton, A. 2008*a*. 3.5 billion years of glass bioalteration: Volcanic rocks as a basis for microbial life? *Earth-Science Reviews*, 89. 156–176.

Staudigel, H., Furnes, H., Mcloughlin, N., Banerjee, N.R., Connell, L.B., Templeton, A., 2008*b*. Microbial glass bioalteration: inferring mechanisms of biocorrosion from trace fossil morphology. *Geochimica et Cosmochimica Acta*, 72, (12), A893.

Stroncik, N.A., Schmincke, H.-U., 2002. Palagonite - a review. *Int J Earth Sci (Geol Rundsch)* 91, 680–697.

Stumm, W. and Morgan, J.J., 1996. Aquatic Chemistry, 3rd edn. John Wiley, New York. 1040 pp.

Thorseth, I.H., Pedersen, R.B., Christie, D.M., 2003. Microbial alteration of 0-30-Ma seafloor and sub-seafloor basaltic glasses from the Australian Antarctic Discordance. *Earth Planet. Sci. Lett*. 215, 237–247.

Toramaru, A., Harada, T., Okamura, T., 2003. Experimental pattern transitions in a Liesegang system. Physica D. 183, 133–140.

Varnavas, S.P., Cronan, D.S., 2005. Submarine hydrothermal activity off Santorini and Milos in the Central Hellenic Volcanic Arc: a synthesis. Chemical Geology. 224, 40–65.

Vollrath, S., Behrends, T., Koch, B.C., Cappellen, P.H., 2013. Effects of temperature on rates and mineral products of microbial Fe(II) oxidation by Leptothrix cholodnii at microaerobic conditions Geochimica et Cosmochimica Acta. 108, 107–124.

Witten, T. A., and Sander, L. M., 1983. Diffusion limited aggregation. Physics Review B. 27, 5686–5697.

Zierenberg R. A. and Schiffman P., 1990. Microbial control of silver mineralization at a seafloor hydrothermal site on the northern Gorda Ridge. Nature. 348, 155–157.